Available online at www.sciencedirect.com

ScienceDirect

IFAC PapersOnLine CONFERENCE PAPER ARCHIVE

IFAC PapersOnLine 59-8 (2025) 237–242

Dynamics and motion-planning for microfluidic flow within elastic walls

Timo Ströhle * **Nicolas Petit** *

* *Centre Automatique et Systèmes (CAS), Mines Paris, Université PSL, 75006 Paris, France (e-mail: timo.strohle@minesparis.psl.eu and nicolas.petit@minesparis.psl.eu).*

Abstract: The article examines the pressure-controlled dynamics of the flowrate in an elastic microchannel. As shown by numerical simulations, the elasticity of the channel gives rise to a complex and nonlinear transient response. The employed numerical scheme is based on the method of characteristics. It is also used to solve the inverse problem of determining the inlet pressure required to achieve a smooth flowrate at the microchannel outlet.

Keywords: flow-control, microfluidics, fluid-structure-interaction

1. INTRODUCTION

Microfluidics is the science of manipulating and controlling fluids at Reynolds numbers lower than 1.0, in very small amounts (microliters to picoliters), in networks of channels with dimensions significantly below 1 mm. It has applications in various fields of science and engineering, including, among others, biology, chemistry and medicine, see e.g. Tabeling (2023); Kirby (2010).

Microfluidic devices often exhibit some elasticity. Unintentional sources of elasticity include compressible air inlets (bubbles) trapped within the device, and compliances of the materials used to produce chips (mostly polydimethylsiloxane (PDMS)). Another common source of elasticity is the compliance of silicone connectors and tubing, which are often preferred over stainless steel versions for their affordability and ease of integration.

The negative effects of elasticities in microfluidics are similar to those created by parasitic impedances in electronic circuits and are primarily noticeable and harmful during transient modes. Many microfluidics applications are plagued with lags in responses, poorly damped oscillations, and difficult to handle water-hammer effects (see e.g. Squires and Quake (2005)). A notable challenge is the difficulty in predicting the total amount of fluid delivered at the circuit's outlet when elasticity is involved. This is a critical issue for all drug delivery applications (see Alavi et al. (2024)).

The article studies the particular issues caused by elastic walls in pressured-based controlled microfluidics and proposes a way to mitigate their detrimental effects. Interestingly, a closely related topic (the transport of fluid in elastic tubes) has been a seminal subject of study since the early days of fluid mechanics. The review article Tijsseling and Anderson (2012) provides a comprehensive summary of important classical models and practical observations, focusing on the pioneering works of Moens and Korteweg (1878) regarding the propagation of pressure waves in unsteady pipe flows within *macroscopic* elastic tubes.

The scenario considered in the article involves a pressurized cavity connected to a downstream microchip via an elastic tube, see Fig. 1. When the pressure is changed, the flowrate at the microchip's inlet (i.e., the flowrate at the system's outlet) becomes unsteady. Unless the pressure variation (input variable) is particularly slow, the flowrate (output variable) exhibits an undesirable overshooting transient before eventually stabilizing. The aim of the article is to address the motion planning problem—specifically, to determine an input transient that ensures the output achieves a smooth and monotonic increase.

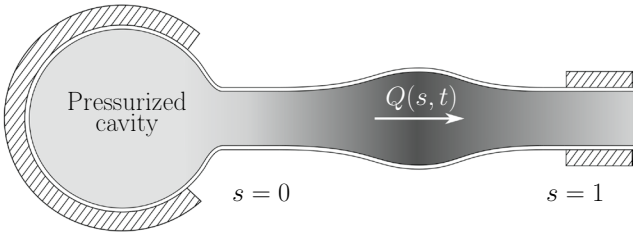

Fig. 1. An incompressible fluid flows from a pressurized cavity to a downstream microchip through an elastic tube.

The article is organized as follows. First, the model of the (incompressible) fluid - (elastic) structure interaction is presented in Sec. 2. The derivation of the governing equations is based on integrating the continuity and Navier-Stokes equation over the cross-sectional area. The resulting equations are additionally subjected to an algebraic equation that relates the pressure to the deformation of the compliant tube (Barnard et al. (1966), Formaggia et al. (2003)). In Sec. 3, we develop a characteristics method to numerically determine the response of the system. In Sec. 4 we report numerical results of this approach, stressing the nonlinear nature of the system observed in the overshoot

10.1016/j.ifacol.2025.08.097

and oscillations of the output of the system when the input changes are gradually increased. In Sec. 5 we employ the characteristics method to solve the inverse control problem. It appears that the input has to overshoot so that the output does not, and that the propagation delay has to be accounted for in form of an anticipation in the control actuation. Finally, conclusions and prospects on future works will be drawn in Sec. 6.

Funding. Timo Ströhle is financially supported by the Deutsche Forschungsgemeinschaft (DFG) through the Walter Benjamin-program. This support is gratefully acknowledged.

2. MODEL

2.1 Physics and balance equations

Consider a compliant vessel with circular cross section containing an incompressible fluid. The system parameters are the time and space varying flowrate $Q(s,t)$ and cross sectional area $A(s,t)$, distributed along the one-dimensional s-axis, with unit length $s \in [0,\,1]$. They are governed by the balance of linear momentum

$$\partial_t Q + \alpha \partial_s \left(\frac{Q^2}{A}\right) + \frac{A}{\rho}\partial_s P + K\frac{Q}{A} = 0\,, \tag{1}$$

where ρ is the mass density, α is the momentum correction factor and K is the friction coefficient, see Formaggia et al. (2003) and the continuity equation

$$\partial_t A + \partial_s Q = 0\,. \tag{2}$$

To close the system, the *tube-law* f relates the luminal pressure $P(s,t)$ relative to the extraluminal pressure P_{ext} to the value of $A(s,t)$

$$P(s,t) = \beta(s)\, f(A(s,t)) + P_{ext}\,. \tag{3}$$

The factor $\beta(s)$ accounts for the geometrical and material properties that influence the stiffness of the tube. Both f and β are derived by considering the radial deformation of a (thick-walled in all generality) tube yielding (see Ströhle and Petit (2025b), Formaggia et al. (1999))

$$f(A) = A^{\frac{1}{2}} - A_0^{\frac{1}{2}}\,, \tag{4}$$

where A_0 is a reference cross sectional area. In this paper we investigate the important case of thin-walled vessels (see Formaggia et al. (1999)). In this context the $\beta-$function can be stated as

$$\beta(s) = \frac{4\sqrt{\pi}(Eh)(s)}{3A_0}\,, \tag{5}$$

where the Young's modulus E and the wall thickness h are, in all generality, depending on s, to account for the different constituent materials of the vessel [1].

After inserting the partial derivative of (3) w.r.t. s, $\partial_s P = f(A)\frac{d\beta}{ds}(s) + \beta\frac{df}{ds}(A)\partial_s A$, some calculus turn (1) into

$$\partial_t Q + 2\alpha\frac{Q}{A}\partial_s Q + g(Q,A)\partial_s A + K\frac{Q}{A} + \frac{A}{\rho}f(A)\frac{d\beta}{ds}(s) = 0\,, \tag{6}$$

where

$$g(Q,A) = \frac{A}{\rho}\beta\frac{df}{dA}(A) - \alpha\left(\frac{Q}{A}\right)^2\,. \tag{7}$$

[1] see again Ströhle and Petit (2025b) for a general expression of β in the case of thick walls.

The pressure in the cavity is controlled using a high-bandwidth pressure controller, as described in Tabeling (2023), resulting in a deformation at the inlet of the vessel. We note the *control* variable [2] $u(t) = A(0,t)$. The outlet of the vessel is connected to a rigid material, s.t. $A(1,t) = \bar{A}$ where $\bar{A}$ is a given constant [3]. The *output* of interest is the flowrate at the outlet $y(t) = Q(1,t)$.

2.2 Summary of the model

Equations (2) and (6) can be seen as a system of coupled first order quasilinear partial differential equations with state $z = (Q, A)^T$

$$\partial_t z + B\partial_s z = C \tag{8}$$

with

$$B = \begin{bmatrix} 2\alpha\dfrac{Q}{A} & g(Q,A) \\ 1 & 0 \end{bmatrix},\; C = \begin{bmatrix} -K\dfrac{Q}{A} - \dfrac{A}{\rho}f(A)\dfrac{d\beta}{ds}(s) \\ 0 \end{bmatrix},$$

subjected to initial conditions $z(s,0) = z_0(s)$, i.e.

$$Q(s,0) = Q_0(s) \quad \text{and} \quad A(s,0) = A_0(s)\,, \tag{9}$$

and boundary conditions

$$u(t) = A(0,t) \quad \text{and} \quad A(1,t) = \bar{A}\,. \tag{10}$$

The output of the system is

$$y(t) = Q(1,t)\,. \tag{11}$$

2.3 Definition of steady-state

To get insight into the dynamics of the system, we illustrate below a steady regime $(Q^{\text{eq}}, A^{\text{eq}})$ obtained for a particular value of the input. At steady-state case, one has $\partial_t Q^{\text{eq}} = 0$ and $\partial_t A^{\text{eq}} = 0$. Continuity equation gives rise to $\partial_s Q^{\text{eq}} = 0$, hence Q^{eq} is uniform. Then, (6) gives

$$g(Q^{\text{eq}}, A^{\text{eq}})\,\frac{dA^{\text{eq}}}{ds} = -K\frac{Q^{\text{eq}}}{A^{\text{eq}}} - \frac{A^{\text{eq}}}{\rho}f(A^{\text{eq}})\frac{d\beta}{ds}\,.$$

This ordinary differential equation (ODE) is readily solved numerically (backwards, staying always from the singularity $A^{\text{eq}} = 0$) from the boundary condition at $s = 1$. A typical example of the vessel shape and the flow regime are pictured in Fig. 2.

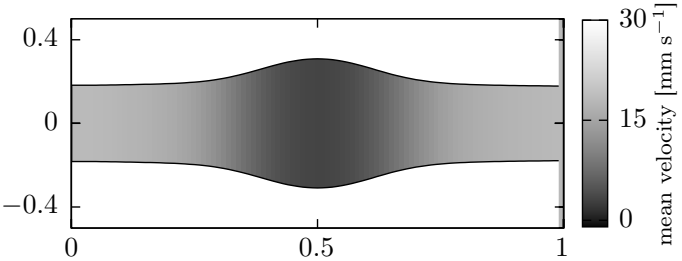

Fig. 2. Deformed vessel and mean velocity $\frac{Q^{\text{eq}}}{A^{\text{eq}}}$ for steady-state flow regime.

3. METHOD OF CHARACTERISTICS

In this section, we exploit the classic *method of characteristics* (see e.g. (Abbott, 1966, Chap. 3),(Courant and Hilbert,

[2] (3) shows the equivalence of $A(0,t)$ and the inlet pressure $P(0,t)$.
[3] or a function of time without loss of generality

1937, Chap. V. §.3 and §.5), Courant and Hilbert (1962)) on the two-dimensional system of quasilinear partial differential equations with non-zero forcing terms (8). We identify the eigenvalues of the matrix B to obtain two scalar ODEs, one for each direction with non-zero right hand-side.

In details, to obtain the ODEs, the method introduces a characteristic $s = k(t)$ where k is the solution of $\det H = 0$ with $H \triangleq B - I\frac{d}{dt}k(t)$. This gives two solutions. Then, the ODEs are obtained as the unique independent line in the matrix $\hat{H}$ defined by exchanging one column of H by the right-hand side of the modified Eq. (12) below. Consider a characteristic line $s = k(t)$ along which $z = z(k(t), t) = \zeta(t)$ is given. Using (8) along with $\partial_t z + \partial_s z \frac{d}{dt}k(t) = \frac{d}{dt}\zeta(t)$, gives

$$\left[B - I\frac{d}{dt}k(t)\right]\partial_s z = C - \frac{d}{dt}\zeta(t) \tag{12}$$

which involves H defined above. The conditions

$$\det(H) = 0 \qquad \text{and} \qquad \det(\hat{H}) = 0\,, \tag{13}$$

are referred to as *directionality* and *compatibility* condition, respectively. Eq. $(13)_1$ has two solutions

$$\frac{d}{dt}k_\pm(t) = \alpha\frac{Q}{A} \pm c, \text{ where } c = \sqrt{\frac{\beta}{2\rho}\sqrt{A} - (1-\alpha)\alpha\left(\frac{Q}{A}\right)^2}\,. \tag{14}$$

Along each of these two lines the solution is governed by compatibility condition $(13)_2$

$$\frac{dQ}{dt} - \left(\alpha\frac{Q}{A} \mp c\right)\frac{dA}{dt} = -K\frac{Q}{A} - \frac{A}{\rho}f(A)\frac{d\beta}{ds}(s)\,. \tag{15}$$

The resulting system of ODEs (15) can be solved numerically (see Sec. 4 and Sec. 5).

4. DIRECT SIMULATION

Problem 1. (Direct problem). Let $\Omega = S \times \mathcal{T}$, where $S = [0, 1] \subset \mathbb{R}$ and $\mathcal{T} = [0, \infty) \subset \mathbb{R}_+$, be the space-time domain of interest and $\partial\Omega_0 = S \times \{0\}$, $\partial S_0 = \{0\} \times \mathcal{T}$ and $\partial S_1 = \{1\} \times \mathcal{T}$ its boundaries. Find the output $y : \partial S_1 \mapsto \mathbb{R}$ with given initial and boundary conditions $z_0 : \partial\Omega_0 \mapsto \mathbb{R}^2$ and $u : \partial S_0 \mapsto \mathbb{R}$ as well as $\bar{A} : \partial S_1 \mapsto \mathbb{R}$ such that (8) is satisfied.

The resolution methods works by defining a stack of slabs in Ω, see Fig. 3. These slabs are defined as follows. Starting from a meshed (non-characteristic) curve $\partial\Omega_{n-1}$, the boundary $\partial\Omega_n$ is defined by the set of points of second intersection of all positive characteristic lines $k_+(t)$ with negative characteristic lines $k_-(t)$ or boundary ∂S_1^n as well as the points of second intersection of all negative characteristic lines $k_-(t)$ with positive characteristic lines $k_+(t)$ or the boundary ∂S_0^n. The space-time strip Ω_n is then defined by the polygon inside $\partial\Omega_{n-1}$, ∂S_0^0, $\partial\Omega_n$ and ∂S_1^n. The numerical method is initialised by defining equidistantly distributed points on the boundary $\partial\Omega_0$. Then the system of ODEs (14) and (15) is discretised in Ω_0 along characteristic lines, that originate at these prescribed points, by applying appropriate finite difference schemes. The system of ODEs (14) and (15) is discretised in Ω_0 along characteristic lines by applying appropriate finite difference schemes. In the context of this work, the implicit midpoint rule and the implicit Euler method have been implemented. Then, the given boundary and initial conditions can be applied directly at the corresponding nodes of the characteristic net. The resulting algebraic system of nonlinear equations can then be solved iteratively for the nodal unknowns of the slab by applying Newton's method. For accuracy and numerical efficiency the Jacobian of this system of equations is calculated analytically.

Thus, by knowing the initial conditions Q and A on $\partial\Omega_0$ along with the knowledge of A at ∂S_0^0 and ∂S_1^0 the solution can be computed on $\partial\Omega_1$. This procedure can be carried out recursively for the space-time slabs Ω_n for $n \in [1, N] \subset \mathbb{N}$, where N indicates the total number of space-time slabs (see Fig. 3 for an illustration thereof). The CFL-condition (see e.g. Allaire (2007)) is fulfilled by construction. In the discretisation, a variable time step is implicitly and adaptively determined by directionality condition (14) depending on the fixed number of nodes. The code is available on the repository (Ströhle and Petit (2025a)).

Fig. 4 reports a numerical error analysis. The error is computed by comparing a steady-state solution of the output that is computed at the last node on ∂S_1 i.e. $y_s = y(t = t_N^*)$, with a numerical solution $y_M(t_N^*)$ depending on the spatial refinement and computed at the same node, i.e. $\varepsilon(M) = \frac{|y_M - y_s|}{|y_s|}$. As expected, see e.g. Leimkuhler and Reich (2004), the error is quadratic with M the number of nodes in space on $\partial\Omega_0$ for the implicit midpoint-rule. One can note that this approach is fundamentally different to the more classical method of (horizontal) lines (see e.g. (Ascher and Petzold, 1998, e.g. Ex.1.7)), where the governing partial differential equation is integrated first in space by means of finite elements followed by an integration in time mostly based on appropriate finite difference schemes.

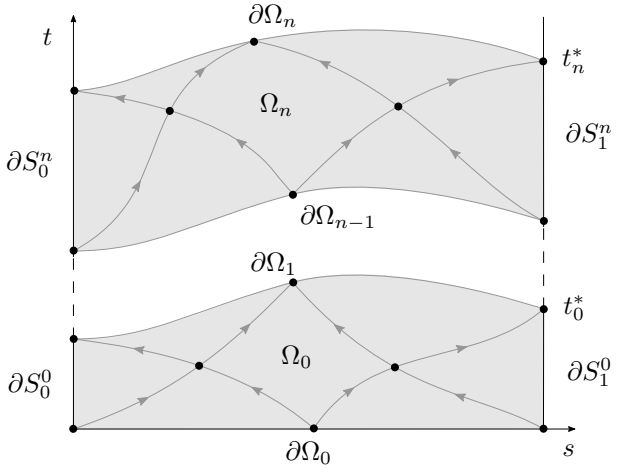

Fig. 3. Illustration of the numerical scheme proposed in Sec. 4 for integrating the direct problem along characteristic lines.

Example 2. Problem 1 is solved with $\alpha = 1.0$, $K = 200$ mm^2 s^{-1} and $\rho = 10^{-6}$ kg mm^{-3}, $A_0 = 0.1$ mm^2. The $\beta-$function is illustrated in Fig 5, implying that the vessel is less stiff in its middle.

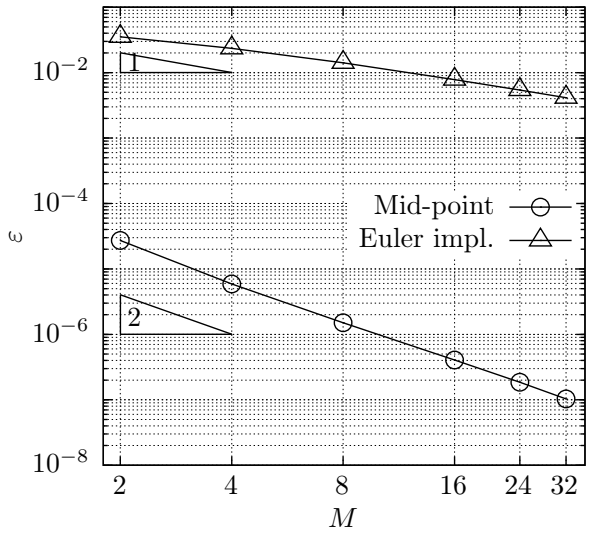

Fig. 4. Numerical error analysis: The accuracy of the proposed method of characteristics achieved by integrating the underlying equations numerically by means of the implicit mid-point rule compared to the implicit Euler method.

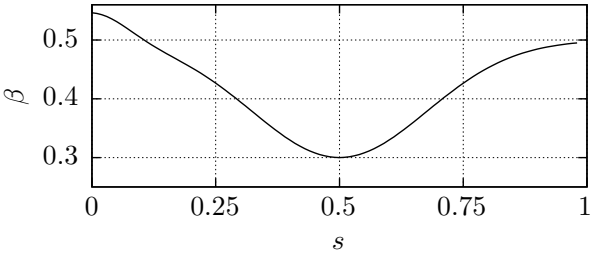

Fig. 5. Illustration of the variation of the stiffness of the vessels wall.

The fluid is initially at rest, i.e. the flowrate is null $Q(.,0) = 0.0$ and the cross-sectional area is being set uniformly to $A(.,0) = A_0$. A smooth monotonically increasing (pressure) input is imposed over some finite time so that

$$u(t) = \begin{cases} \dfrac{\Delta A(0)}{2}\left(\cos\left((\gamma+1)\pi\right)+1\right) + A_0 & \text{for } t_0 < t > T \\ A_0 & \text{for } t < t_0 \\ A_0 + \Delta A(0) & \text{for } t > T\,, \end{cases} \tag{16}$$

where $\gamma(t) = \frac{1}{2}\cos\left(\left(\frac{t-t_0}{T}+1\right)\pi\right)+\frac{1}{2}$ s.t. the system is being transferred after the time $T = 10.0$ ms from an initial steady-state $[0\ A_0]^T$ at time $t_0 = 0$ to another steady-state $[Q(.)\ A_0 + \Delta A(.)]^T$ with $\Delta A(0) = 0.01$ mm^2. Fig. 6 stresses that the input-output response system is nonlinear. The response of the output according to the prescribed inputs of varying amplitudes is shown. Fig. 7 stresses the laggy output response, and the transient overshoot of the inlet flowrate, temporarily filling the volume corresponding to the expansion of the vessel. These numerical results have been obtained by employing 15 nodes initially equally distributed on $\partial\Omega_0$. On average, 5 Newton iterations for each space-time slab were required to converge quadratically to the presented numerical solution, i.e. to achieve an Euclidean norm of the residual vector, that is smaller than a given tolerance $\varepsilon = 10^{-8}$.

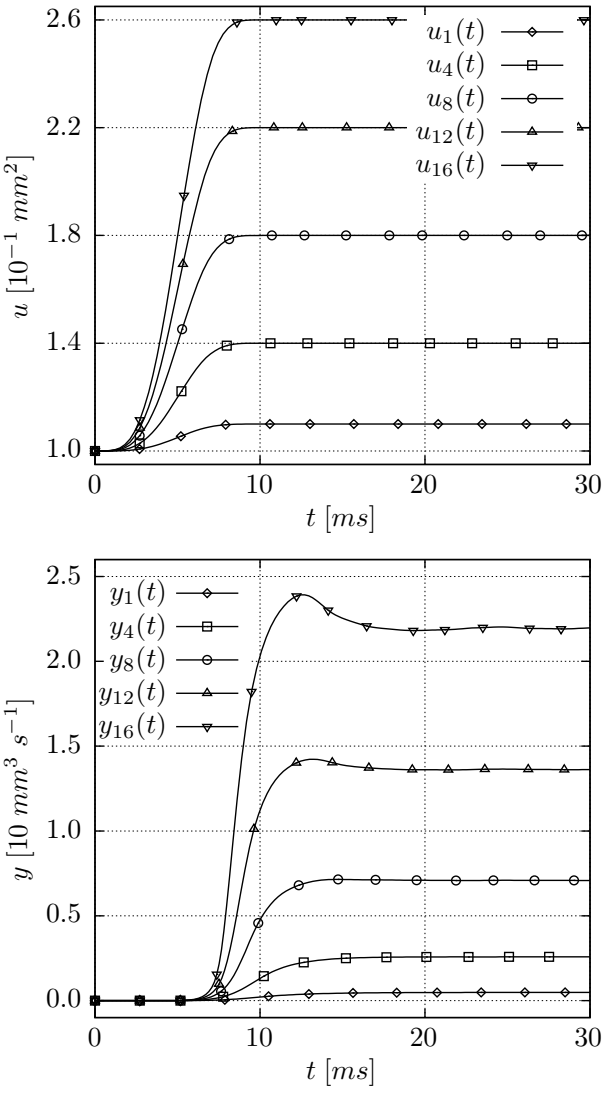

Fig. 6. Input-output response: Illustration of different imposed inputs $u_i(t)$ with $\Delta A_i(0) = i \cdot \Delta A(0)$ (top) and the corresponding outputs $y_i(t)$ (bottom).

5. MOTION-PLANNING

We now employ the characteristic method of Sec. 3 to solve the following inverse problem.

Problem 3. (Motion-planning). With the notations of Problem 1. Consider a sufficiently smooth $y : \partial S_1^* \mapsto \mathbb{R}$ for $\partial S_1 \supset \partial S_1^* = \{1\}\times[t_0^* > 0, \infty)$ along with given initial and boundary conditions $z_0 : \partial\Omega_0 \mapsto \mathbb{R}^2$ and $\bar{A} : \partial S_1 \mapsto \mathbb{R}$, find the input $u : \partial S_0 \mapsto \mathbb{R}$ such that (8) is satisfied.

The transformation of the PDEs at hand into a system of ODEs along characteristic lines enables a construction of a numerical scheme, that is capable of solving Problem 3 by connecting the boundaries through characteristic lines along which the information flows. With the notations of Problem 3, assume that $\partial\Omega_0$ is non-characteristic, i.e. that there exist no characteristic line $k^{\pm}(t)$ which lies on $\partial\Omega_0$. Along with given boundary conditions for $A(1,t) = \bar{A}(t)$

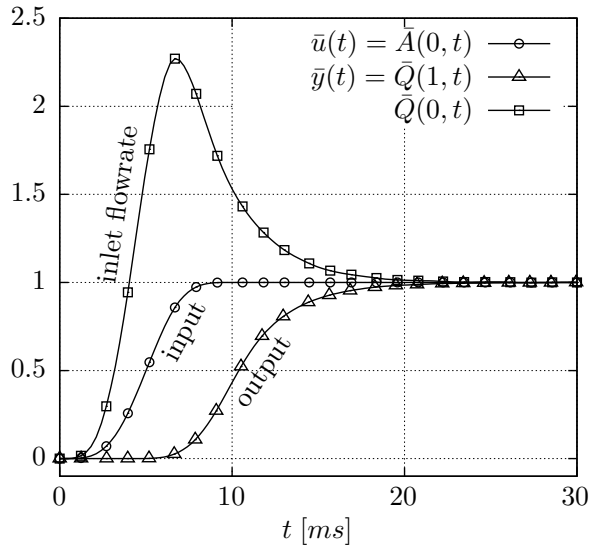

Fig. 7. Numerical results of the normalised output $\bar{y}(t) = Q(1,t)\ Q^{-1}(1,\infty)$ along with the normalised flow rate $\bar{Q}(0,t) = Q(0,t)\ Q^{-1}(1,\infty)$ according to the normalised prescribed input $\bar{u}(t) = \bar{A}(0,t) = (A(0,\infty) - A(0,0))^{-1}(A(0,t) - A(0,0))$

.

on $\partial S_1^0 = \{1\} \times [0, t_0^*]$, that need to be chosen consistently with respect to the given initial conditions, i.e. $\bar{A}(t{=}0) = A_0(s{=}1)$, the solution at any grid point within the space-time triangle Ω_0 (defined by the three boundaries $\partial\Omega_0$, ∂S_1^0 and k_0^+ (see Fig. 8)), is fully determined by the system of ODEs (14) and (15) along characteristic lines $k^{\pm}$.

Once the solution is computed at every grid points in Ω_0, a prescribed output can be defined on the time interval $\mathcal{T}^* = \partial S_1 \setminus \partial S_1^0 = [t_0^*, \infty)$ s.t. $y : \mathcal{T}^* \mapsto \mathbb{R}$ is fulfilling the condition $y(t_0^*) = Q(1, t_0^*)$. This is a necessary condition for the prescribed output. Then, the solution within space-time slabs Ω_n, $n \in [1, N]$ (where N indicates the number of space-time slabs) can be computed recursively by solving (14) and (15) in accordance with the previously computed solution at points along $k_{n-1}^{\pm}$ as initial condition together with the prescribed output y and the cross-sectional area $\bar{A}$ at the boundary ∂S_1^n. The numerical scheme is illustrated in Fig. 8.

A delay between the input and output signal is visible in Fig. 7. It is here determined numerically, and is implicitly taken into account by the motion planning method. This task is not straightforward due to the nonlinearity of the equations at hand, resulting in a dependence of the delay on the input signal itself. This situation is often observed in systems subjected to *hydraulic delay* see e.g. Clerget and Petit (2020); Bekiaris-Liberis et al. (2024). The delay $D(t)$ of the response of the output $y(t)$ to the input $u(t - D(t))$ is therefore determined implicitly by the characteristic lines k^+, i.e.

$$1 = \int_{t-D(t)}^{t} k'_+(t)\ \mathrm{t}\ . \tag{17}$$

The presented solution strategy takes this delay implicitly into account. Note that the initialisation procedure does not depend on the imposed output. So, if the initial conditions do not change, this procedure only needs to be executed once before planning different manoeuvers using the recursive procedure stated above.

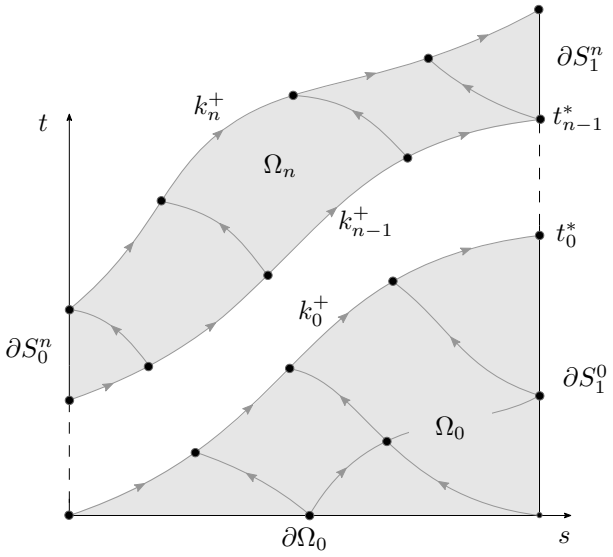

Fig. 8. Illustration of the numerical scheme proposed in Sec. 5 for solving the motion-planning problem by inverse integration along characteristic lines.

Remark 4. (Parameterisation) Within each space-time slab $\Omega_n \forall n \in [1, N] \subset \mathbb{N}$ the input can be parameterised by the prescribed output. According to Fig. 9, the solution at point O_n^1 depends on the solution at points O_{n-1}^0 and O_n^0, which is given by the boundary conditions $(10)_2$ and (11). Once the solution is calculated at the point O_n^1 and since the solution along k_{n-1}^+ is known the solution at the points O_n^m is determined by the solution at points O_n^{m-1} and O_{n-1}^{m-1} for all $m \in [2, M] \subset \mathbb{N}$, where M indicates the number of nodes on k^+, (cf. Fig. 9). Thus, the solution in ∂S_0, including the unknown input $u(t) = A(0,t)$, can be completely parameterised by the solution given at ∂S_L, including the output $y(t) = Q(1,t)$.

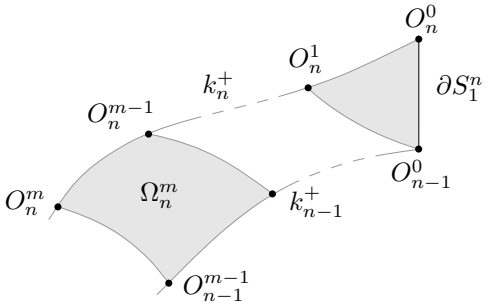

Fig. 9. Parameterisation of the governing equations along characteristic lines within the space-time slab Ω_n.

Example 5. The system described in Ex. 2 is reconsidered. The output is prescribed according to (16) by replacing A_0 and $\Delta A(0)$ with $Q_0(1)$ and $\Delta Q(1)$, respectively. Furthermore t_0 and T are set to 5 ms and 15 ms, respectively.

The results of the numerical simulations are summarised in Fig. 10. Therein the flowrate at the boundaries is plotted together and compared with the input. Note that, at an expense of a moderate increase of the input signal compared to Fig.7, the output is significantly sped-up. The

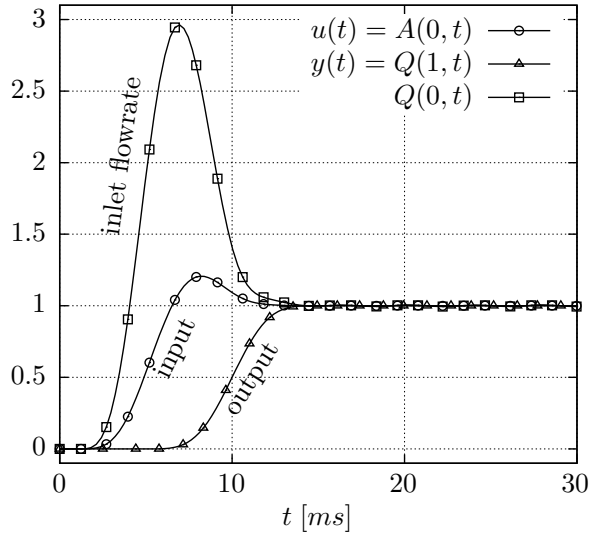

Fig. 10. Numerical results of the normalised input $\bar{u}(t) = (\Delta A(0))^{-1}\ (A(0,t) - A_0)$ along with the normalised flow rate $\bar{Q}(0,t) = Q(0,t)(Q^{\text{eq}})^{-1}$ according to the normalised prescribed output $\bar{y}(t) = \bar{Q}(1,t) = Q(1,t)\ (Q^{\text{eq}})^{-1}$. Q^{eq} is the corresponding steady-state solution.

desired output flowrate is reached fast and in finite time thanks to the pressure input signal carefully calculated using the method outlined above.

These numerical results have been obtained by employing 15 nodes equally distributed on $\partial\Omega_0$. On average, 4 Newton iterations for each space-time slab were required to reach the presented numerical solution.

6. CONCLUSION

The aim of this research was to investigate the flow control problem of incompressible flow in compliant tubes for microfluidic applications. Due to the hyperbolic structure of the governing equations, a numerical method based on the classical *method of characteristics* was developped and applied for direct simulation and resolution of the inverse problem (motion-planning).

In this context we could observe phenomenologically and analytically that the mode and magnitude of the expansion of the tube, i.e. the increase in volume of the fluid inside the tube, has an effect on the delay. For example, lower stiffness leads to greater hydrodynamic capacitance and therefore greater delays. Especially for the inverse problem, the influence of the hydrodynamic capacitance on the delay plays a crucial role. This analysis and numerical investigations has enabled to reveal and specify necessary conditions for the prescribed output and its feasible range. These conditions are induced by the velocity of wave propagation and have been implicitly incorporated in the numerical scheme presented.

Among the limitations of this work is that the scheme does not yet allow the treatment of shocks, i.e. crossing characteristic lines leads to a failure of the computations. One further interesting direction that would be worth investigating is the question of finding a time-optimal input to transfer the system from one steady state to another, under flowrate constraints, while avoiding shocks. Furthermore, when dealing with varying parameters, a model predictive control should be established to ensure a robust control. The codes for direct simulation and motion planning are available on GitHub (see Ströhle and Petit (2025a)).

REFERENCES

Abbott, M. (1966). *An Introduction to the Method of Characteristics*. Elsevier, NY.

Alavi, S.E., Alharthi, S., Alavi, S.F., Alavi, S.Z., Zahra, G.E., Raza, A., and Shahmabadi, H.E. (2024). Microfluidics for personalized drug delivery. *Drug Discovery Today*, 29(4), 103936.

Allaire, G. (2007). *Numerical analysis and optimization: an introduction to mathematical modelling and numerical simulation*. OUP Oxford.

Ascher, U. and Petzold, L. (1998). *Computer methods for ordinary differential equations and differential-algebraic equations*. SIAM.

Barnard, A., Hunt, W., Timlake, W., and Varley, E. (1966). A theory of fluid flow in compliant tubes. *Biophysical Journal*, 6(6), 717–724.

Bekiaris-Liberis, N., Bresch-Pietri, D., and Petit, N. (2024). Compensation of input-dependent hydraulic input delay for a model of a microfluidic process under zweifach–fung effect. *Automatica*, 160, 111428.

Clerget, C.H. and Petit, N. (2020). Optimal control of systems subject to input-dependent hydraulic delays. *IEEE Trans. Autom. Control*, 66(1), 245–260.

Courant, R. and Hilbert, D. (1937). *Methoden der mathematischen Physik II*. Springer-Verlag.

Courant, R. and Hilbert, D. (1962). *Methods of Mathematical Physics II*. Wiley-Interscience, New York.

Formaggia, L., Lamponi, D., and Quarteroni, A. (2003). One-dimensional models for blood flow in arteries. *Journal of Engineering Mathematics*, 47, 251–276.

Formaggia, L., Nobile, F., Quarteroni, A., and Veneziani, A. (1999). Multiscale modelling of the circulatory system: a preliminary analysis. *Computing and Visualization in Science*, 2, 75–83.

Kirby, B.J. (2010). *Micro- and nanoscale fluid mechanics: transport in microfluidic devices*. CUP Cambridge.

Leimkuhler, B. and Reich, S. (2004). *Simulating Hamiltonian Dynamics*. Cambridge University Press.

Squires, T.M. and Quake, S.R. (2005). Microfluidics: Fluid physics at the nanoliter scale. *Reviews of modern physics*, 77(3), 977–1026.

Ströhle, T. and Petit, N. (2025a). Flow-control: Modelling, simulation and control of the flow of incompressible fluids in compliant vessels, github-repository. URL `https://github.com/timostroehle/flow-control`.

Ströhle, T. and Petit, N. (2025b). Notes on the deformation of thick-walled vessels due to transmural pressure changes. Preprint available at: `https://github.com/timostroehle/flow-control`.

Tabeling, P. (2023). *Introduction to microfluidics*. OUP.

Tijsseling, A. and Anderson, A. (2012). A. Isebree Moens and D. J. Korteweg: On the speed of propagation of waves in elastic tubes. In *BHR Group - 11th International Conferences on Pressure Surges*, 227 – 245.